Volume 14
Number 13
7 April 2022
Pages 4773-5250

Nanoscale

rsc.li/nanoscale

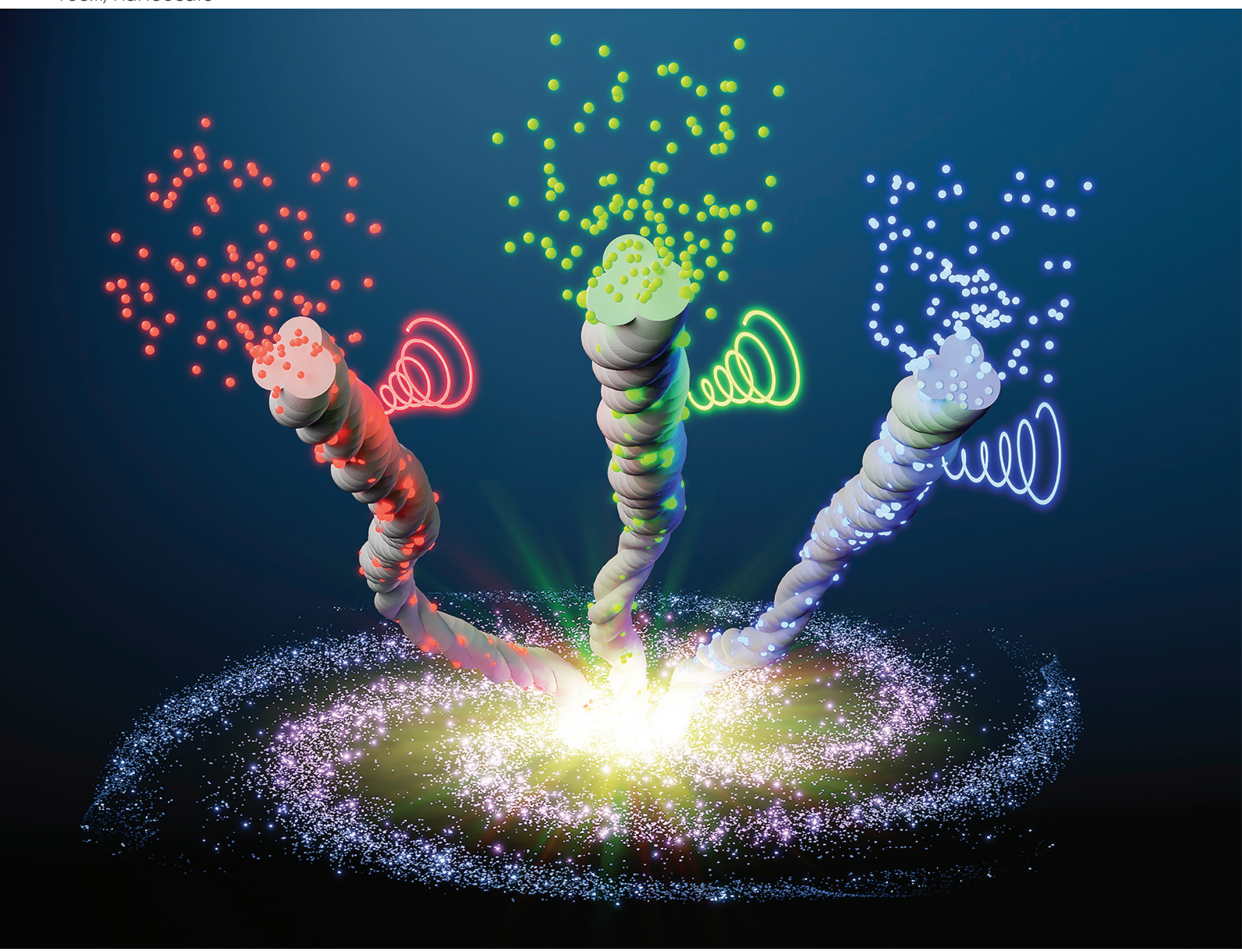

ISSN 2040-3372

ROYAL SOCIETY OF CHEMISTRY

PAPER
Jatish Kumar *et al.*
Mandelic acid appended chiral gels as efficient templates for multicolour circularly polarized luminescence

NCNST

Nanoscale

PAPER

View Article Online
View Journal | View Issue

Cite this: *Nanoscale*, 2022, **14**, 4946

Mandelic acid appended chiral gels as efficient templates for multicolour circularly polarized luminescence†

Kumbam Lingeshwar Reddy, ‡[a] Jikson Pulparayil Mathew, ‡[a] Sonia Maniappan, [a] Catherine Tom,[b] Elizabeth Shiby, [a] Ravi Kumar Pujala [b] and Jatish Kumar *[a]

Mandelic acid is a medicinally important chiral molecule that is widely used as a vital component in antibiotics, antiseptics and cosmetics. While the medicinal properties of mandelic acid are well known, its aggregation and gelation characteristics, which are crucial to finding applications as cosmetics and ointments, are least explored. We have designed and synthesized a pair of mandelic acid derivatives and investigated their aggregation properties in binary solvent mixtures. The compounds undergo self-assembly through various noncovalent interactions, leading to the formation of robust chiral gels. Strong birefringence could be visualised from the individual structures constituting the gel. The large rod-like chiral structures are utilized as efficient templates for the assembly of ultra-small luminescent achiral carbon nanodots. The transfer of optical activity from the chiral host matrix to the fluorescent guest nanoparticles resulted in the generation of circularly polarized luminescence signals from the hybrid nanocomposites. The use of blue, green and red-emitting nanodots led to the fabrication of multicolour chiral light-emitting materials capable of covering the entire visible range. Considering the numerous medicinal benefits offered by mandelic acid and carbon nanodots, the materials constituting the nanocomposites, the distinct dimensions presented in the current work open new avenues for chiral light emitting materials to be used in biomedical research.

Received 29th December 2021,
Accepted 6th February 2022

DOI: 10.1039/d1nr08506a

rsc.li/nanoscale

Introduction

Supramolecular gels formed by the self-assembly of low molecular weight organogelators are gaining vast attention in multiple research areas ranging from bionanomaterials and drug delivery systems to electronic devices, light-emitting materials and templates for the assembly of nanostructures.[1–3] Organized structures formed through noncovalent interactions between the molecules render these materials with intriguing properties.[4,5] The information hoarded in the individual components can be transferred/enhanced in the assembled structures.[6,7] In this regard, exploitation of the supramolecular gels as templates for the incorporation of nanomaterials leading to hybrid composite materials is of particular interest. The composition of the gels is a key factor that needs attention when employing such materials for application in pharmaceutical or biomedical research.[8,9] Alpha hydroxy acids (AHAs) are a group of nontoxic natural acids commonly used as skin moisturizers and for treating ailments related to skin.[10] Mandelic acid (MA) is a common AHA that is not only used for skin remedies but also as an antibiotic and antiseptic agent.[11] It has also been used as an antibacterial agent and for the treatment of urinary tract infections.[12–14] One of the most important benefits of MA is that it is gentler on skin compared to other AHAs making it the ideal choice for people with sensitive skin. MA also improves skin appearance as it promotes collagen production, a main protein found in skin and connective tissue.[15,16] While the benefits of MA are numerous, this class of compounds have not been explored for their gel forming abilities. Herein we design a pair of MA derivatives that undergoes self-assembly in suitably selected binary solvent mixtures leading to the formation of strong organogels.

Another important property of MA that has been least explored is its chiral character. Optical activity in molecules and materials is a research area that is gaining relevance in recent years due to its diverse applications.[17] The chirality of individual components can be amplified through the self-

[a]*Department of Chemistry, Indian Institute of Science Education and Research (IISER) Tirupati, Tirupati, Andhra Pradesh-517507, India.*
E-mail: jatish@iisertirupati.ac.in
[b]*Department of Physics, Indian Institute of Science Education and Research (IISER) Tirupati, Tirupati, Andhra Pradesh-517507, India*

†Electronic supplementary information (ESI) available. See DOI: 10.1039/d1nr08506a

‡These authors contributed equally to the work.

assembly of molecules. Host–guest interactions are simple and effective strategies wherein self-assembled aggregates can function as chiral templates to induce optical activity into achiral moieties.[18–20] Induction of ground state chirality into achiral materials thereby generating induced circular dichroism (CD) signals has been actively studied.[21–24] In this regard, a relatively new concept that reveals the chiral information in the excited state is the circularly polarized luminescence (CPL).[25–28] CPL investigates the differential emission in left- and right-circularly polarized light, and has gained enormous attention in last decade due to its wide potential in diverse fields such as information storage, chemical sensors, stereoscopic displays and photodynamic therapy.[29] These applications require that the materials fulfil two major criteria; (i) a large luminescence dissymmetry factor (g_{lum})[30] and (ii) multicolour emission.[31] Energy/charge transfer,[32,33] supramolecular self-assembly[25,34] and doping of liquid crystals[35] are some of the common approaches adopted for the amplification of g_{lum}. However, achieving consistent CPL from molecules and materials has remained a challenging task. With an aim to utilize the optical activity of the MA-based organogels, we have adopted a host–guest approach wherein the chirality of host can be transferred into an achiral guest moiety leading to multicolour CPL. A combination of MA-based chiral gel and achiral luminescent carbon nanodots (CNDs) could function as the host–guest system generating chiral light emission, the intensity and wavelength of which could be modulated based on the chiroptical features of the constituent elements.

Results and discussion

The gelator molecules with varying chain lengths were synthesized by reacting L and D-isomers of MA with alkyl diamine (Fig. 1 & S1†). The protocol adopted for the synthesis of the C-12 derivative is outlined in Fig. 1. Two equivalents of MA (one of the enantiomers) was coupled with 1,12-diaminododecane in presence of EDC, HOBt and a base to obtain the product *N*,*N*′-(dodecane-1,12-diyl)bis(2-hydroxy-2-phenylacetamide) (compound **1**). The obtained product was purified and characterized using ^{1}H NMR, ^{13}C NMR and mass spectrometry (Fig. S2–S4†). The molecule comprises of two MA units at the ends separated by a long alkyl chain. The alkyl chain renders hydrophobicity whereas the MA unit bestows the molecule with functionalities that can enhance intermolecular interactions. Functional groups on MA along with the lone pairs of electrons (on oxygen and nitrogen) can facilitate hydrogen bonding leading to the self-assembly of the molecules in suitably selected solvents. The chiral center on MA can induce optical activity to the molecular system. The chiral nature of the synthesized compound was established from the CD spectral studies. Mirror image signals with intense positive and negative peaks corresponding to the n–π* transition (225–235 nm) was observed for pure **1*R*** and **1*S*** respectively (Fig. 2a). Mirror image CD profile due to the π–π* transition was also observed for the enantiomers in the 260–280 nm spectral range (inset, Fig. 2a).[36] The peaks matched well with the absorption profile of the monomeric form of the molecule (Fig. S5†).

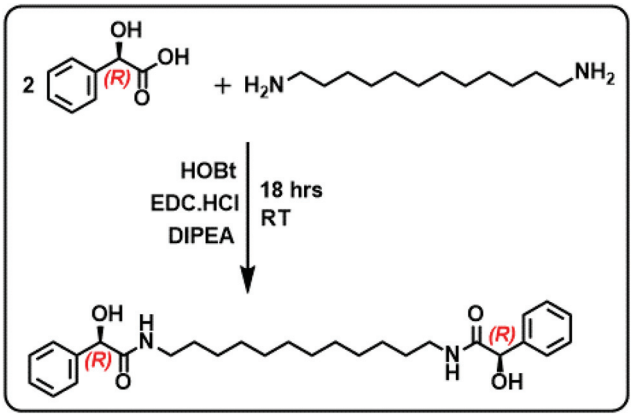

Fig. 1 Scheme illustrating the synthesis of compound **1*R***.

To investigate the self-assembly and the subsequent gelation properties of **1*R***, the solubility of the compound was studied in different solvent combinations (Table S1†). Compound **1** was found to be highly soluble in organic solvents like DMF, DMSO and THF. The compound exhibited solubility in ethanol and methanol upon sonication and heating. Thus, DMF and DMSO were chosen as good solvents to solubilize the compound and analyse its gelation properties. The UV-visible absorption spectra of compound **1*R*** in DMF exhibited a peak around 270 nm corresponding π–π* transition of the aromatic ring.[36] Sequential addition of the universal solvent, water, resulted in the decrease in the intensity of the peak at 270 nm with the concomitant formation of a new peak at 305 nm (Fig. 2b). The bathochromic shift in the peak position is indicative of the self-assembly of the molecules through π stacking of the benzene rings.[37,38] Further increase in com-

Jatish Kumar

Jatish Kumar obtained his PhD in Chemistry from the CSIR-National Institute for Interdisciplinary Science and Technology (NIIST), Trivandrum, India. After completion of his PhD, he worked initially as JSPS postdoctoral fellow and later as an assistant professor at the Nara Institute of Science and Technology (NAIST), Nara, Japan. Later he moved as a Marie Curie postdoctoral fellow to CIC biomaGUNE in San Sebastian, Spain. He joined the Indian Institute of Science Education and Research (IISER) Tirupati, India as Assistant Professor in December 2018. His research interests are in the field of nanoscale chirality, photochemistry and assembly of nanomaterials.

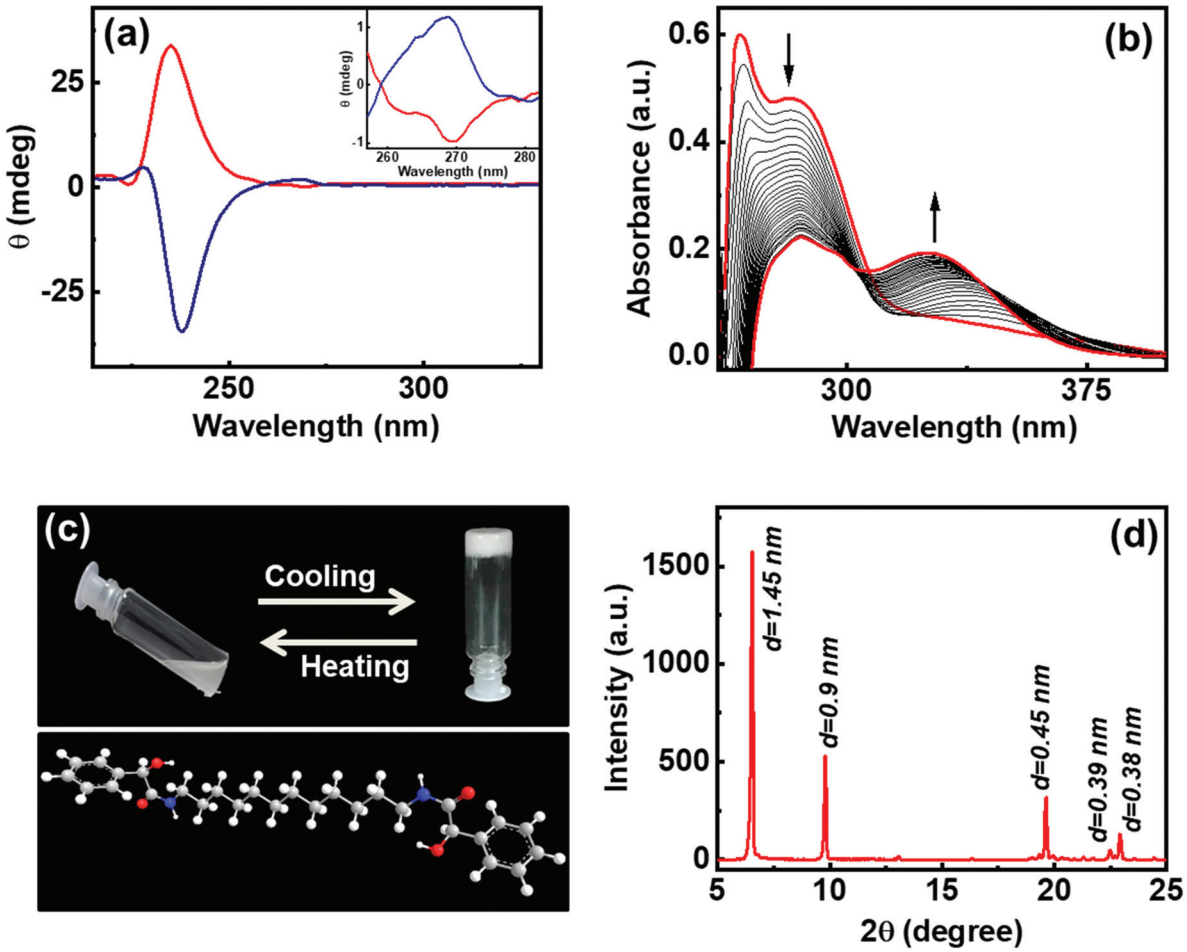

Fig. 2 (a) CD spectra of **1*R*** (red trace) and **1*S*** (blue trace) in ethanol. Inset shows the enlarged CD peaks in the 257–283 nm spectral range. (b) UV-vis absorption spectral changes of **1*R*** in DMF (4.4 mM) upon stepwise addition of water (0 to 700 μL). (c) Photographic images of temperature-controlled sol–gel transformation of **1*R*** (4 wt%). The 3D representation of the compound is also shown. (d) PXRD spectrum of the lyophilized gel formed from **1*R***.

position of water resulted in a white turbid solution. Gelation was observed in a solvent composition of 4 : 1 of DMSO/DMF : H_2O at a concentration of 4.0 wt% of **1*R***. The white gel undergoes transformation from gel phase to solution state upon heating, and the gel phase is restored upon further cooling of the solution to room temperature, typical properties exhibited by organogels (Fig. 2c). The lyophilized samples were subjected to powder X-ray diffraction (PXRD) analysis. Sharp XRD peaks indicated the well-defined arrangement of molecules in gel phase (Fig. 2d). The XRD data exhibited diffraction peaks at 2θ = 6.65, 9.79, 19.64, 22.48 and 22.9 degrees corresponding to a *d*-spacing of 1.45, 0.9, 0.45, 0.39 and 0.38 nm, respectively. Diffraction peaks corresponding to a *d* spacing of 0.45 nm and 0.39 nm can be ascribed to the hydrogen bonded β sheet like arrangement of the molecules.[39,40] The peak corresponding to a *d* spacing of 0.38 nm can be attributed to the weak π–π interaction between the aromatic groups,[40–42] and the peak at 0.9 nm could be assigned to the spacing between the layers.[43] The XRD pattern showed no peaks corresponding to molecular chain lengths. However, peaks were observed for smaller values indicating that the self-assembled structures in **1** are made up from the interdigitated layered structures.[39] Hence, the XRD data suggests that the noncovalent interactions operative between the molecules play a significant role in the formation and sustenance of the supramolecular assembly.

The intermolecular interactions play a crucial role in deciding the nature of aggregates formed during the self-assembly. The molecular interactions that occur during the gelation can be verified with the help of ^{1}H NMR titration studies. Upon addition of D_2O to compound **1** dissolved in DMSO-d_6, there occurs a shift in the position of the NMR peaks. The peaks corresponding to OH and NH protons exhibited a linear progressive downfield shift with increasing D_2O fraction (Fig. 3a). This is the result of a charge depletion around the hydrogen atom suggesting the formation of H-bonding between the molecules.[44] Moreover, a doublet to singlet transformation was observed in the peak at δ = 4.88 ppm confirming the involvement of hydroxyl proton in hydrogen bonding (Fig. 3b). The upfield shift of the aromatic protons and the alkyl protons at

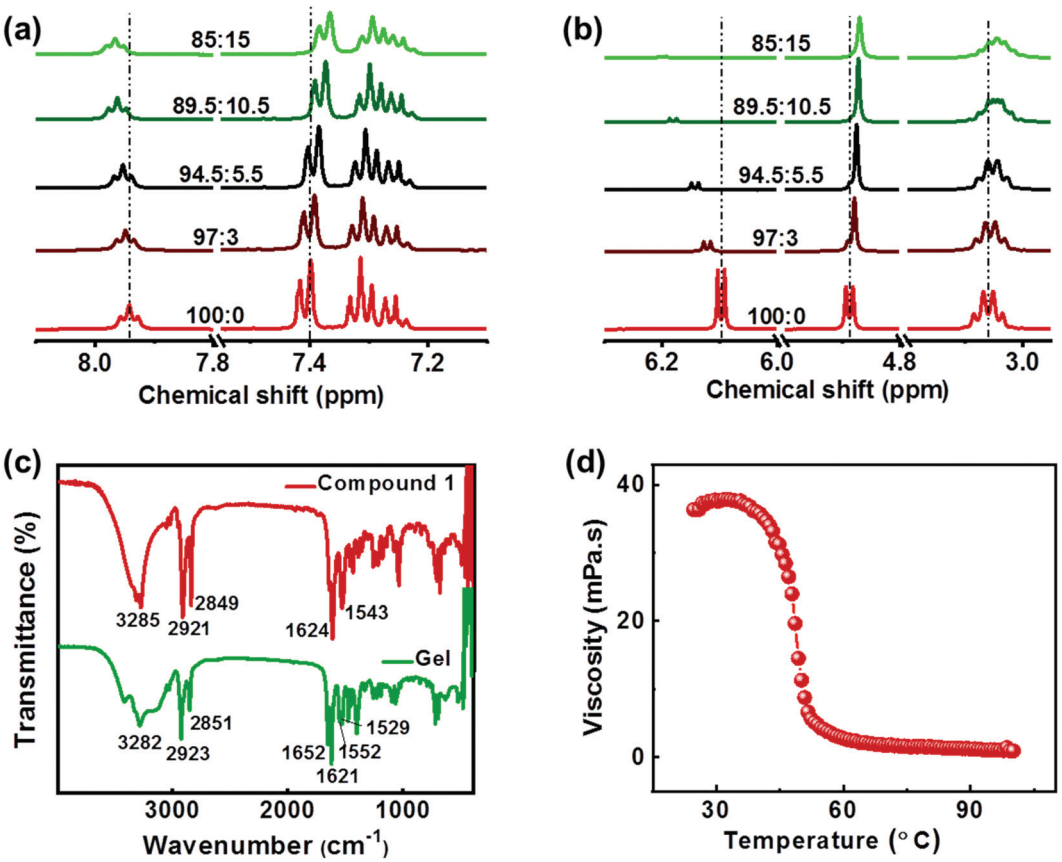

Fig. 3 (a and b) ^{1}H NMR spectral shifts observed upon stepwise addition of D_2O to **1*R*** dissolved in DMSO-d_6. The spectral shifts corresponding to (a) NH and aromatic protons, and (b) OH, chiral CH and aliphatic protons. (c) FT-IR spectra of crude (red trace) and the lyophilised gel (green trace) of **1*R***. (d) Temperature dependent viscosity changes of gel formed from **1*R*** (4 wt%) in a binary solvent mixture of DMSO and water (4 : 1).

4.88 ppm, 3.05 ppm and in the 1.0–1.5 ppm indicates the presence of non-covalent interactions between the molecules (Fig. 3b & S6†). The shift in the aromatic peaks is an indication of the π–π interaction and the changes in the aliphatic region points to the role of hydrophobic interactions between the alkyl chains during the self-assembly of molecules.[38,45] The Fourier transform infrared (FTIR) spectra of the crude sample **1** and that of the lyophilized gels were compared to study the intermolecular interactions. The FTIR characteristics of the crude compound showed broad peak at 3285 cm^{-1} corresponding to the vibrational frequencies of O–H and N–H stretching (Fig. 3c). Peaks corresponding to the amide I (due to carbonyl C═O stretching) and amide II (C–N stretching in combination with N–H bending) bands were observed at 1624 cm^{-1} and 1543 cm^{-1} respectively. In contrast, the lyophilized gel exhibited a broadening of O–H peak indicating the presence of hydrogen bonding. Appearance of two peaks at 1552 cm^{-1} and 1529 cm^{-1} compared to a single peak at 1543 cm^{-1} in crude sample implies the presence different modes of N–H bending due to hydrogen bonding. Moreover, the shift of the C═O stretching peak to 1621 cm^{-1} confirms the formation of intermolecular hydrogen bonding with carbonyl groups. Similar studies on self-assembled structures have reported the alteration of the amide I bond (predominantly C═O) in case of any possible hydrogen bonding.[46,47] Based on the XRD, NMR and FTIR results, it can be inferred that the gelation of the compound is an outcome of various intermolecular forces operating between the molecules; (i) amide and hydroxy groups facilitating the hydrogen-bonding, (ii) aromatic rings undergoing π–π stacking interactions, and (iii) the long alkyl chains enabling hydrophobic interactions, leading to self-assembly of the molecule in a suitably selected solvent system.

Investigations were carried out to analyse the viscosity of the gel as a function of temperature. The sample containing 4 wt% of **1*R*** when subjected to heating showed no appreciable changes at low temperatures (Fig. 3d). However, a gradual decrease in viscosity was observed beyond 35 °C followed by a sharp drop around 40 °C. Almost 10-fold reduction in viscosity was observed between 40 °C and 55 °C with a critical gelation temperature of 48.5 °C. The studies reinforce the typical nature of gelators; high viscosity at low temperatures whereas transformation to free-flowing liquid at high temperature as shown in Fig. 2c. Further, variable temperature NMR studies were employed to probe (i) the role of intermolecular interactions in the self-assembly and (ii) to analyse the stability of

the aggregated structures at high temperature. An increase in temperature from 298 K to 358 K exhibited trends opposite to that observed during aggregation (*vide supra*). Prominent upfield shifts were observed in the amide and hydroxy protons upon increasing temperature indicating the breakage of hydrogen bonds (Fig. S7†). A gradual downfield shift (though of lesser amplitude) was observed in the aliphatic and aromatic protons confirming the loss of π–π stacking and hydrophobic interactions. The change in chemical shift is an indication of the loss of intermolecular interactions and the disassembly of aggregates into their monomer constituents at high temperature. The results further emphasize the role of various noncovalent interactions in the self-assembly of the molecule in DMSO/water mixture. The molecular interactions remain intact at low temperatures whereas the aggregated structures breakdown above the gel melting temperature resulting in a free-flowing liquid.

Visual insight into the morphological features of the gel can be obtained through optical and electron microscopic imaging. Polarized optical microscope (POM) images of gel samples at different concentrations were taken by placing polarizer and analyser parallel (PPL) and perpendicular (XPL-cross polarizers) to each other (Fig. 4 & S8†). The optical microscopic images showed network-like structures. When placed in PPL position, the analyser doesn't allow the light to pass through the sample. As the samples were placed in between cross polarizers, coloured patterns were visible due to the birefringence exhibited by the gels. As the concentration of the gel increases, the network becomes stronger and shows strong birefringent behaviour (Fig. 4d & S8†). Hence, the structural anisotropies in the material are evident from the birefringence property exhibited by the gels. Further, the diluted samples were visualised under cross polarisers and lambda plates (Fig. 4e and f). The elongated particles were clearly visible, and birefringence could be observed from individual structures indicating highly oriented molecular arrangement in the self-assembled aggregates. While the chiral nature is faintly visible in the elongated particles, a thorough investigation is needed to further understand these aspects.

Understanding the finer structural details is important in analysing the morphology of nanostructures constituting the

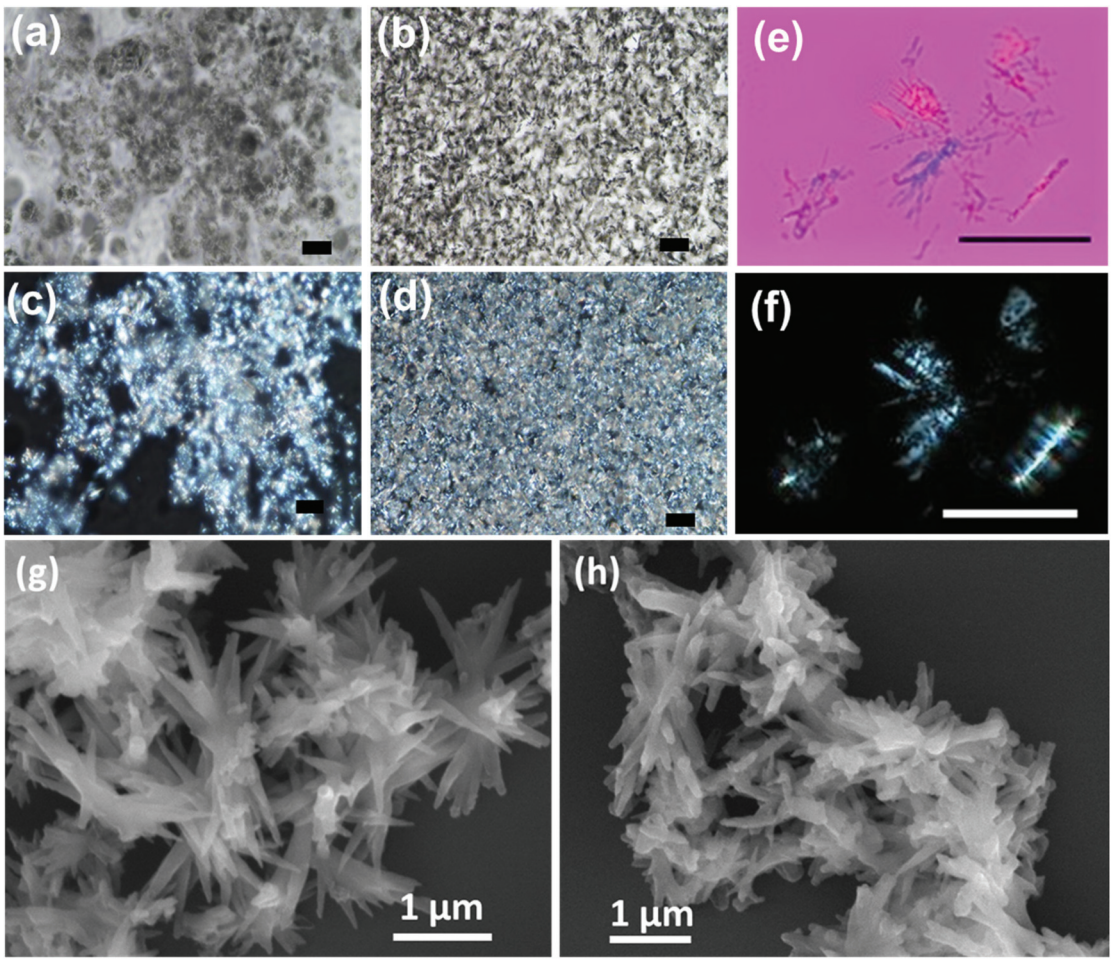

Fig. 4 POM images of **1*R*** in (a and b) PPL and (c and d) (XPL cross polarizer) configurations for (a and c) 2.0 and (b and d) 6.3 wt% of the gel samples (scale bar = 100 μm). POM images of the diluted samples of **1*R*** collected with (e) lambda plate and cross polarizers and (f) cross polarizers only (scale bar = 50 μm). FE-SEM images of organogels formed from (g) **1*R*** and (h) **1*S***.

gel. Field emission scanning electron microscopy (FE-SEM) was employed as a powerful tool to analyse the structural composition of the gel. The FE-SEM images of the gels showed elongated needle/plate-like structures that were a few micrometres in length (Fig. 4g and h). Dimensions of few micrometres for the assembled structures demonstrate a long-range order. The nanostructures were interlinked resulting in a 3D network structure that can effectively entrap solvents in it. Similar structures were observed for the gels formed from both **1*R*** and **1*S***.

Rheological characterizations are means of investigating the viscoelastic properties of the gels. Fig. 5a shows the amplitude sweep plots of gels at different concentrations measured at a constant angular frequency (ω) of 10 rad s^{-1}. For all the samples storage modulus (G') was found to be higher than loss modulus (G'') at low shear strains which indicates that elastic behaviour dominates over viscous nature. However, after cross-over point, $G'' > G'$ indicating the dominance of the liquid nature. G' and G'' is plotted as a function of angular frequency at a constant shear strain (γ) of 1 (Fig. 5b). G' dominates over G'' over the entire frequency range indicating dominance of the elastic behaviour over the viscous behaviour. A gradual increase in the G' value with the increase in weight percentage of the compound indicates that the strength of the gel strongly depends on the concentration of the compound (Fig. 5c). The samples from 2.0 to 6.3 wt% show the strong gel behaviour and G' has weak dependence of angular frequency. The steady state viscosity curves shown in Fig. 5d confirm the shear thinning behaviour of the gels where viscosity decreases with shear rate. Such a behaviour can be modelled by fitting to a power-law, $\eta = k\dot{\gamma}^{n-1}$, where η viscosity k is the flow consistency index and n is the flow behaviour index. If $n = 1$, the sample is a Newtonian fluid and if $n > 1$, it behaves as a shear thickening fluid. However, for $0 < n < 1$, the sample exhibit shear thinning behaviour. The value of n is always less than 1 confirming the shear thinning behaviour of the gels, and the micron sized structures align themselves with the flow field.

From the above discussions, it is evident that the judicious choice of molecular system is important for the formation of strong gels. The designed molecule possesses functionalities having specific role towards gelation. In addition to the hydrogen bonding moieties on MA, the long alkyl chain facilitates

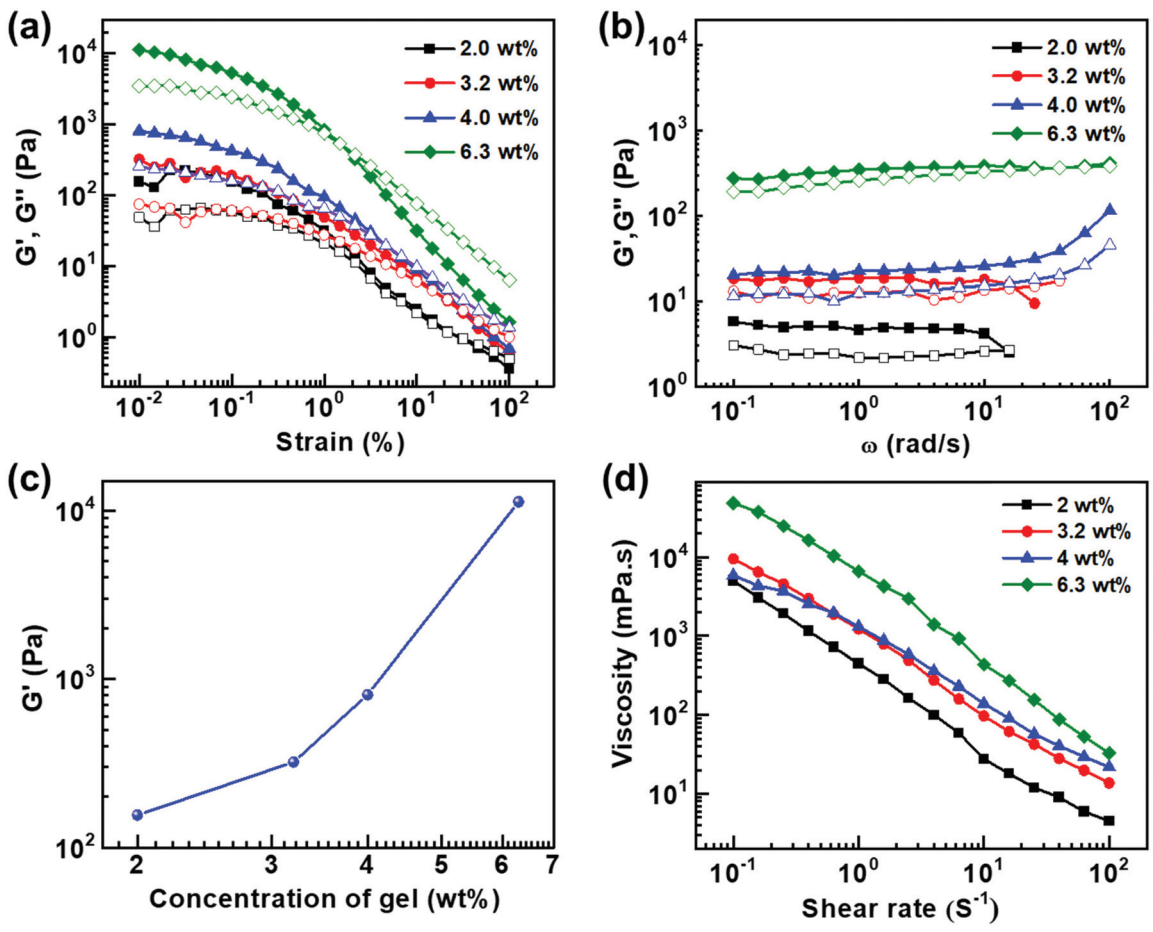

Fig. 5 (a) Amplitude sweep at a fixed ω = 10 rad s^{-1} and (b) frequency sweep at γ = 1 of gel samples at varying concentrations (solid symbols and hollow symbols indicate G' and G'' respectively). (c) Plot of G' *versus* concentration of gel samples at shear strain of 0.01%. (d) Flow curves of gel samples at different concentrations.

hydrophobic interactions between the molecules. Such weak interactions are vital for the self-assembly and the subsequent gelation of the molecule. To understand the role of the van der Waals forces and hydrophobic interactions, we synthesized a control molecule with a shorter C-6 alkyl chain length (**2*R*** and **2*S***) (Fig. S1†). It is observed that **2*R*** do not form stable gels even at higher concentrations of 5.5 wt% (Fig. S9†) further emphasizing the importance of long alkyl chains in promoting the weak van der Waals forces and hydrophobic interactions between molecules thereby inducing self-assembly and gelation properties in the C-12 derivative.

The established properties of the gels formed from **1*R*** and **1*S*** shows that these are materials having potential to be used in diverse fields. One of the applications that can utilize the chiral as well as the gelation properties of the system is to employ these materials as templates for the assembly of nanomaterials thereby generating chiral luminescence. CPL is an important technique having applications in diverse fields ranging from display devices to anti-counterfeiting and chiral sensing.[25–29] Achieving intrinsic chiral emission from nanomaterials has been a challenge. Hence, a distinctive approach is to adopt template assisted methods wherein hybrid structures capable of generating chiral emission are fabricated by the assembly of achiral fluorescent guests onto chiral templates. The efficiency of the chirality transfer will play a crucial role in determining the efficacy of the composite system as chiral light emitting material.[20,48] Moreover, the approach avoids tedious synthetic routes required for the preparation of complex organic systems. In this regard, efforts have been scarce towards achieving multi-colour CPL with reasonably high dissymmetry factors from chiral gels as templates. We devised a strategy wherein MA derived gel acts as the host matrix and multi-coloured CNDs are used as the guest particles. The chirality is derived from the host matrix and the fluorescence stems from the guest particles.

CNDs as luminescent materials possess enormous benefits such as, low production cost, good luminescence quantum yield, stability and biocompatibility.[49–52] The starting material for the synthesis includes chemical compounds like citric acid, urea and ethylenediamine that can provide carbon source. Based on the precursor material, these CNDs show additional benefits in numerous areas. For example, citric acid-based CNDs can act as efficient intracellular reactive oxygen scavengers.[53] It has also been observed that N-doped CNDs act as anti-inflammatory agents, thus enabling faster wound healing.[54] The concept of introducing chirality in CNDs was lately applied by covalently attaching chiral moieties to their surface and by selecting the chiral precursors for the synthesis.[55,56] Here, we employed achiral CNDs as fluorescent materials and incorporated them into the MA based chiral gel to achieve CPL.

Achiral CNDs exhibiting blue, green and red luminescence were prepared by adopting a hydrothermal method using citric acid, urea and ethylene diamine as the precursors in DMSO, DMF and formamide as solvents. All CNDs were purified by adopting dialysis and precipitation methods (details in ESI†). The purified CNDs were analysed using UV-visible and fluorescence spectroscopy. The CNDs showed typical absorption peaks corresponding to the electronic transitions (Fig. 6a). Blue emission was obtained for CNDs synthesized using citric acid dissolved in DMSO whereas CNDs synthesized with citric acid and urea in DMF exhibited green luminescence.[57] Emission colour could be tuned to red for CNDs synthesized using citric acid and ethylene diamine in formamide (Fig. 6b).[58] The relative photoluminescence quantum yield were calculated to be 14.3, 9.9 and 22.2% for the blue, green and red emitting CNDs, respectively (Table S2†). The CNDs were thoroughly characterized by employing various spectroscopic and microscopic techniques. The IR spectra of CNDs exhibited peaks depending on the precursors used for the synthesis (Fig. S10†). The spectral profile showed a good agreement with the reported values. Blue CNDs showed peaks at 3410 cm^{-1}, 2929 cm^{-1}, 1653 cm^{-1}, 1089 cm^{-1}, and 1252 cm^{-1} corresponding to the O–H, C–H, C═O, S═O, and C–O vibrational stretching frequencies respectively, indicating the formation of graphitic carbon core. For green CNDs IR peaks were observed at 3365 cm^{-1}, 3130 cm^{-1}, 1712 cm^{-1}, and 1625 cm^{-1} corresponding to the O–H, N–H, C═O, and C═N vibrational stretching frequencies respectively, which is an indication of the conjugated graphitic structure.[57] Similarly, red CNDs displayed IR peaks at 3381 cm^{-1}, 3139 cm^{-1}, 1639 cm^{-1}, 1380 cm^{-1}, and 1310 cm^{-1} due to the O–H, N–H, C═O, C–N, and C–O vibrational stretching frequencies respectively, indicating the formation of aromatic carbon core.[58] Further characterization was done with the help of X-ray photoelectron spectroscopy (XPS). XPS analysis of the purified samples exhibited peaks at 288, 402 and 533 eV (Fig. S11, S12 & Table S3†), corresponding to the presence of C, N and O respectively, which confirms the formation of CNDs. The excited state lifetimes of the CNDs were analysed using the time correlated single photon counting (TCSPC) experiments. The PL decay curves were fitted by a tri-exponential formula and the lifetimes were in the nanosecond timescale (Fig. S13 & Table S4†), values typically observed for the CNDs.[58] Further, morphological characterization was carried out using transmission electron microscopic (TEM) imaging. TEM images of all the 3 sets of purified CNDs displayed small spherical particles with an average diameter of 2–4 nm (Fig. 6c–e). The presence of small particles confirms the formation of CNDs in solution.

Having characterized the gels as well as the CNDs, the next step is to synthesize hybrid nanocomposites comprising of the chiral template and the luminescent nanoparticle. For achieving this, compounds **1*R*** and **1*S*** were dissolved in solution containing CNDs in DMSO/DMF. To the clear solution, stepwise addition of water resulted in the formation of stable gels wherein the fluorescent nanoparticles were embedded in the gel matrix. On incorporation of CNDs into the organogel, no physical changes were observed in the microstructures constituting the gels as evident from the SEM images (Fig. S14†). We have also investigated the viscoelastic properties of gels before and after the incorporation of CNDs. The amplitude as well as

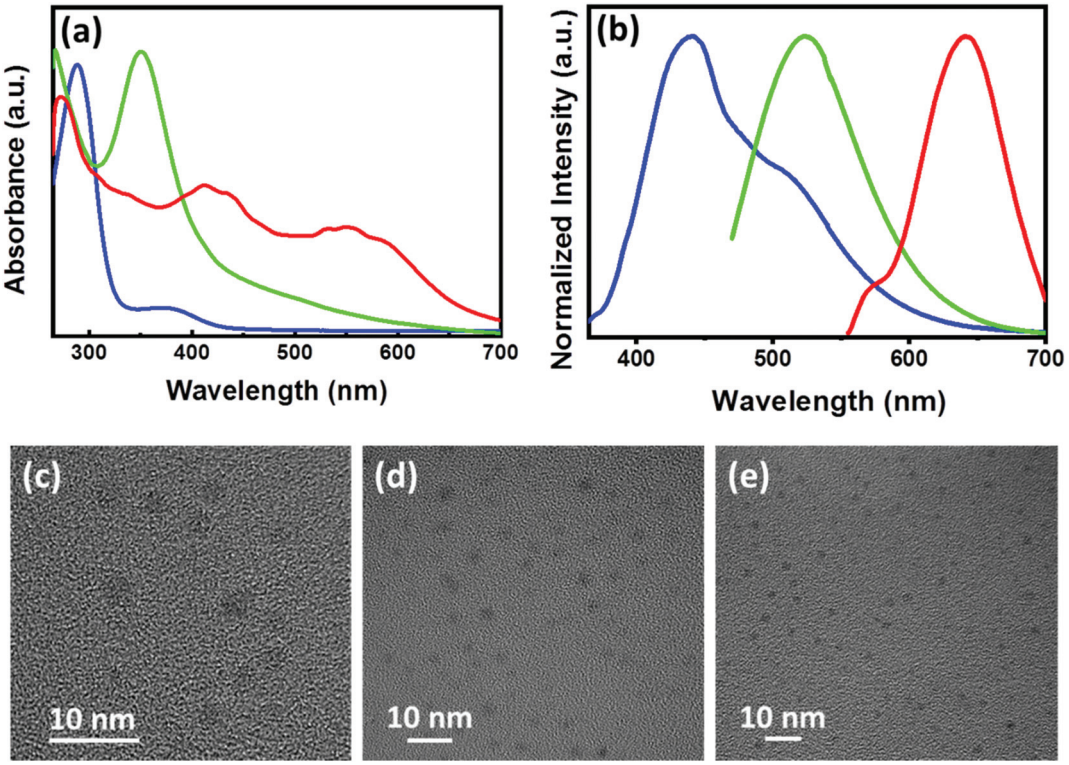

Fig. 6 (a) UV-visible and (b) luminescence spectra of blue, green, and red emitting CNDs (spectra are shown in respective colors). The excitation wavelengths are 350, 455 and 540 nm for the blue, green and red emitting CNDs respectively. (c–e) TEM images of the purified samples of (c) blue, (d) green, and (e) red emitting CNDs.

frequency sweep of the gels carried out in presence of the CNDs showed plots similar to that observed for the samples without CNDs (Fig. S15†). No appreciable changes could be noticed in the viscosity of the gels indicating that the gels remain intact even after the incorporation of the luminescent nanomaterials. Furthermore, CNDs in the gels exhibited triexponential decay with lifetime similar to that observed for the pure CNDs in solution state (Fig. S13 & Table S4†). This indicates that the nanoparticles also retain their inherent luminescence after the formation of hybrid nanostructures. The hybrid composites were subjected to chiroptical analysis. Interestingly, CPL signals could be observed from the blue, green and red regions of the electromagnetic spectrum depending on the nature of CNDs incorporated in the nanocomposites (Fig. 7). Positive and negative signals were observed for the *R* and *S* isomers of the gels. The extent of chiral dissymmetry is quantified using the anisotropic factor represented as $g_{lum} = 2(I_L - I_R)/(I_L + I_R)$, where I_L and I_R are the intensities of left and right-circularly polarized light, respectively.[25,26] The g_{lum} values for the composite system comprising of **1*R*** were found to be -5.7×10^{-3} at 424 nm, -2.4×10^{-3} at 529 nm and -4.5×10^{-3} at 608 nm corresponding to the blue, green and red region of the electromagnetic spectrum. Similar values with reversal in sign were obtained for the corresponding CNDs embedded in chiral gels with opposite handedness (Table S5†). Reproducibility was checked by collecting the CPL spectra from different spots of the sample (Fig. S16†). Consistency in sign of CPL signal and the g_{lum} values emphasised that the signals are due to the chiral emission from the hybrid structures and ruled out the possibility of any artefacts due to linear polarisation effects. Control experiments with pure CND solutions displayed no CPL peaks indicating that the CNDs are inherently achiral in nature (Fig. S17†). The CPL signals in presence of the gel arises due to the interaction of the fluorescent nanoparticles with the chiral surface of the self-assembled structures thereby leading to an efficient chirality transfer from the gel matrix to the CNDs. Thus, we have developed an optically active multicoloured chiral emissive nanocomposite composed of MA-based chiral gel incorporated with citric acid-based CNDs.

One of the challenges in the assembly of nanoparticles in the organogels is to understand the mechanistic details. The nanoparticles can either undergo self-assembly or co-assembly in the chiral gels. We have performed two sets of experiments to check the possibility of co-assembly and the self-assembly of CNDs. In the first set of experiments, the CNDs (in DMF) was added to the molecule in its powder form. The molecule is soluble in DMF and hence, forms a clear solution. Water was then added dropwise to induce gelation. The hybrid gels were subjected to CPL analysis (Fig. S18a†). In the second set, pure gels were synthesized by dropwise addition of water into the molecule dissolved in DMF. This was followed by the addition

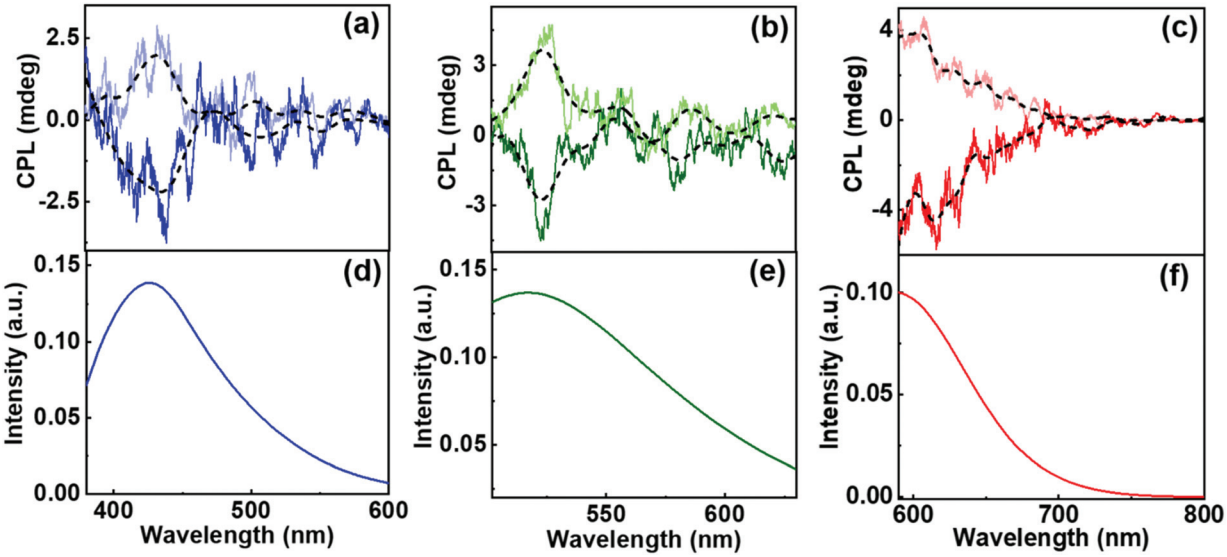

Fig. 7 (a–c) CPL and (d–f) fluorescence spectra from the nanocomposites composed of the (a and d) blue, (b and e) green and (c and f) red emitting CNDs encapsulated in the gels. Dark and light traces correspond to the spectra from CNDs embedded in gels composed of **1*R*** and **1*S*** respectively.

of CND powder. The resulting hybrid gel was thoroughly mixed before subjecting to CPL analysis (Fig. S18b†). CPL signals from the latter would suggest a self-assembly of CNDs on the chiral gel whereas chiral signals from the former can be an indication of either co-assembly or self-assembly. To our surprise, CPL signals were obtained from both sets of experiments, though with slightly varying intensities. These results point more towards the possibility of a self-assembling mechanism. Moreover, the consistency in the images, lifetime and viscoelastic data before and after CND addition to the gel point towards the likelihood of a self-assembling mechanism over the co-assembly (Fig. 8).

All 3 sets of CNDs exhibited excitation dependent fluorescence (Fig. S19†). Excitation dependent luminescence is an interesting phenomenon in CNDs that can be ascribed to the varying particle size distribution, presence of surface oxidation states or different functional groups on the surface.[52] One of the widely accepted mechanisms is the dependence of fluorescence on the degree of surface oxidation. Surface oxidation leads to surface defects that can trap excitons, and recombina-

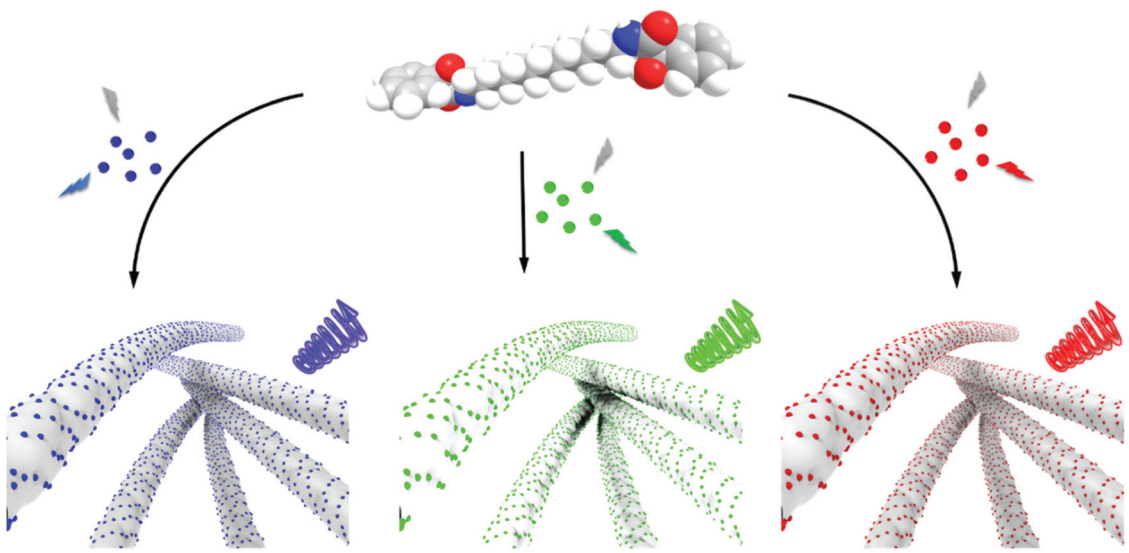

Fig. 8 Scheme illustrating the self-assembly of compound **1** in presence of blue (left), green (middle) and red (right) emitting achiral CNDs. Aggregation is induced in compound **1** in presence of CNDs results in the assembly of the nanoparticles on the surface of molecular aggregates. The chiral host–guest interactions resulting in the generation of right-handed CPL signals is shown.

tion of these trapped excitons causes the red-shift in emission.[52] The presence of different surface functional groups can also introduce diverse fluorophores or emitting states in the CNDs. Another important factor is the existence of different types of aggregations even at very dilute solutions leading to the engrossment of multiple distinct electronic states, which eventually leads to excitation-dependent emission in CNDs.[59] These properties of CNDs were exploited to study the excitation dependent CPL of the synthesized nanocomposites. Achiral red CNDs incorporated into the chiral gel matrix exhibited excitation dependent CPL. Studies revealed that the sample exhibited CPL at 545 nm when excited using 475 nm light whereas CPL was observed at 600 nm for excitation at 540 nm (Fig. S20†). We could successfully demonstrate such large shifts in CPL, which in general is difficult to achieve. Reasonably high g_{lum} values of -6.0×10^{-3} and -4.8×10^{-3} could be attained at 545 and 600 nm respectively for the ***R*** isomer. Thus, multi-colour chiral light emission was achieved by adopting different approaches from the same set of host–guest hybrid nanosystems. The introduction of achiral CNDs as guests onto the surface of chiral supramolecular assemblies acting as host leads to the chirality transfer from the host materials to the guest nanoparticles. The transfer of chirality from the host to guest can occur either through an interaction of the achiral nanoparticles with the optically active units present on the molecule or through the helical arrangement of the nanoparticles along the host template. No chiral signals were observed on mixing CNDs with compound **1** in DMSO/DMF ruling out any chirality transfer from the molecule to the nanoparticles in the monomeric dispersed state (Fig. S21†). Chiral signals emerged only after the addition of water and subsequent gelation of the compound emphasising the role of aggregated structures in inducing the CPL signals. The efficient chirality transfer results in the generation of tunable chiral luminescence from the CNDs, the nature of which can be modulated by varying the guest nanoparticles (Fig. 8). The sign and intensity of CPL is governed by the chirality of the molecular aggregates constituting the template whereas the emission colour is dependent on the luminescence wavelength of the guest nanoparticles. Moreover, the constituents of the composite system, MA and CNDs, possess enormous biological benefits that make the nanohybrids potential candidates for the use as antibacterial and anti-inflammatory agents, and investigations in this direction are in progress.

Conclusions

In summary, we have synthesized a MA based chiral molecule that self-assembles in DMSO/H_2O mixture to form optically active gels that possess high storage modulus and exhibit strong birefringence. Adopting a host–guest approach multi-coloured achiral CNDs could be successfully encapsulated into the chiral gel. The gel constituted of elongated chiral structures that could function as templates assisting the effective interaction of nanoparticles on its surface. The efficient transfer of chirality from the host matrix to the guest CNDs resulted in multi-colour CPL generation from the materials. Based on the type of CNDs embedded in the gel, blue, green and red CPL was generated on excitation using visible light. In addition to the demonstrated application as chiral light emitting materials, due to the numerous advantages offered by MA and CNDs in the biological field, the synthesized chiral nanocomposites hold great potential in the biomedical field to be developed as ointments or skin care lotions.

Conflicts of interest

There are no conflicts to declare.

Acknowledgements

J. K. thank the Department of Science and Technology for the Core Research Grant (DST-SERB project: CRG/2019/002715), and the Council of Scientific and Industrial Research (CSIR project no. 01(3029)/21/EMR-II), Government of India, for funding. K. L. R. acknowledges IISER Tirupati, J. P. M., S. M. and C. T. acknowledge DST-INSPIRE for fellowship. R. K. P. acknowledges the Department of Science and Technology for INSPIRE Faculty Award Grant [DST/INSPIRE/04/2016/002370] and a Core Research Grant (CRG/2020/006281, DST-SERB), Government of India, for funding. The authors acknowledge IISER Tirupati for providing the research facilities. The authors thank Prof. K. George Thomas and Mr Sanoop M. S., IISER Thiruvananthapuram for their generous help with SEM and TEM imaging, lifetime measurements, XPS analysis, and XRD characterization of the samples.

Notes and references

1 S. Banerjee, R. K. Das and U. Maitra, *J. Mater. Chem.*, 2009, **19**, 6649–6687.
2 X. Cao, A. Gao, J.-t. Hou and T. Yi, *Coord. Chem. Rev.*, 2021, **434**, 213792.
3 E. Busseron, Y. Ruff, E. Moulin and N. Giuseppone, *Nanoscale*, 2013, **5**, 7098–7140.
4 S. S. Babu, V. K. Praveen and A. Ajayaghosh, *Chem. Rev.*, 2014, **114**, 1973–2129.
5 B. R. Madhanagopal, J. Kumar and K. N. Ganesh, *Nanoscale*, 2020, **12**, 21665–21673.
6 M. G. F. Angelerou, P. W. J. M. Frederix, M. Wallace, B. Yang, A. Rodger, D. J. Adams, M. Marlow and M. Zelzer, *Langmuir*, 2018, **34**, 6912–6921.
7 S. Dhiman, A. Sarkar and S. J. George, *RSC Adv.*, 2018, **8**, 18913–18925.
8 D. Wang, G. Tong, R. Dong, Y. Zhou, J. Shen and X. Zhu, *Chem. Commun.*, 2014, **50**, 11994–12017.
9 A. R. Hirst, B. Escuder, J. F. Miravet and D. K. Smith, *Angew. Chem., Int. Ed.*, 2008, **47**, 8002–8018.

10 P. Babilas, U. Knie and C. Abels, *J. Dtsch. Dermatol. Ges.*, 2012, **10**, 488–491.
11 C. Zhu, X. Lin, J. Wu and Y. Wei, *Anal. Sci.*, 2002, **18**, 1055–1057.
12 A. Wójcik, M. Kubiak and H. Rotsztejn, *Postepy Dermatol. Alergol.*, 2013, **30**, 140–145.
13 J.-M. Jeon, H.-I. Lee, S. G. Kim, S.-H. Han and J.-S. So, *Food Sci. Biotechnol.*, 2010, **19**, 583–587.
14 M. Motamedifar, A. Bazargani, E. Sarai and H. Sedigh, *World Appl. Sci. J.*, 2014, 31.
15 S. W. Jacobs and E. J. Culbertson, *Facial Plast. Surg.*, 2018, **34**, 651–656.
16 B. Edison, H. Smith, W.-H. Li, R. Parsa, B. Green, P. Konish, M. Dufort and N. Tierney, *J. Am. Acad. Dermatol.*, 2020, **83**, AB97.
17 V. Kuznetsova, Y. Gromova, M. Martinez-Carmona, F. Purcell-Milton, E. Ushakova, S. Cherevkov, V. Maslov and Y. K. Gun'ko, *Nanophotonics*, 2021, **10**, 797–824.
18 X. Yan, T. R. Cook, J. B. Pollock, P. Wei, Y. Zhang, Y. Yu, F. Huang and P. J. Stang, *J. Am. Chem. Soc.*, 2014, **136**, 4460–4463.
19 M. Golla, S. K. Albert, S. Atchimnaidu, D. Perumal, N. Krishnan and R. Varghese, *Angew. Chem., Int. Ed.*, 2018, **58**, 3865–3869.
20 S. Maniappan, S. B. Jadhav and J. Kumar, *Front. Chem.*, 2021, **8**, 557650.
21 R. Thomas, J. Kumar, J. George, M. Shanthil, G. N. Naidu, R. S. Swathi and K. G. Thomas, *J. Phys. Chem. Lett.*, 2018, **9**, 919–932.
22 H. Zhu, Q. Li, Z. Gao, H. Wang, B. Shi, Y. Wu, L. Shangguan, X. Hong, F. Wang and F. Huang, *Angew. Chem., Int. Ed.*, 2020, **59**, 10868–10872.
23 P. K. Sukul, P. K. Singh, S. K. Maji and S. Malik, *J. Mater. Chem. B*, 2013, **1**, 153–156.
24 E. Severoni, S. Maniappan, L. M. Liz-Marzán, J. Kumar, F. J. G. de Abajo and L. Galantini, *ACS Nano*, 2020, **14**, 16712–16722.
25 J. Kumar, T. Nakashima and T. Kawai, *J. Phys. Chem. Lett.*, 2015, **6**, 3445–3452.
26 J. P. Riehl and F. S. Richardson, *Chem. Rev.*, 1986, **86**, 1–16.
27 E. M. Sánchez-Carnerero, A. R. Agarrabeitia, F. Moreno, B. L. Maroto, G. Muller, M. J. Ortiz and S. de la Moya, *Chem. – Eur. J.*, 2015, **21**, 13488–13500.
28 F. Zinna and L. Di Bari, *Chirality*, 2015, **27**, 1–13.
29 Y. Sang, J. Han, T. Zhao, P. Duan and M. Liu, *Adv. Mater.*, 2020, **32**, 1900110.
30 M. Xu, X. Wu, Y. Yang, C. Ma, W. Li, H. Yu, Z. Chen, J. Li, K. Zhang and S. Liu, *ACS Nano*, 2020, **14**, 11130–11139.
31 H. Shang, Z. Ding, Y. Shen, B. Yang, M. Liu and S. Jiang, *Chem. Sci.*, 2020, **11**, 2169–2174.
32 D. Yang, P. Duan, L. Zhang and M. Liu, *Nat. Commun.*, 2017, **8**, 15727.
33 J. Han, D. Yang, X. Jin, Y. Jiang, M. Liu and P. Duan, *Angew. Chem., Int. Ed.*, 2019, **58**, 7013–7019.
34 Y.-X. Yuan, M. Hu, K.-R. Zhang, T.-T. Zhou, S. Wang, M. Liu and Y.-S. Zheng, *Mater. Horiz.*, 2020, **7**, 3209–3216.
35 B. A. San Jose, J. Yan and K. Akagi, *Angew. Chem., Int. Ed.*, 2014, **53**, 10641–10644.
36 A. C. Evans, A. S. Petit, S. G. Guillen, A. J. Neukirch, S. V. Hoffmann and N. C. Jones, *RSC Adv.*, 2021, **11**, 1635–1643.
37 J. Xiao, X. Xiao, Y. Zhao, B. Wu, Z. Liu, X. Zhang, S. Wang, X. Zhao, L. Liu and L. Jiang, *Nanoscale*, 2013, **5**, 5420–5425.
38 M. Kumar and S. J. George, *Nanoscale*, 2011, **3**, 2130–2133.
39 K. Basu, N. Nandi, B. Mondal, A. Dehsorkhi, I. W. Hamley and A. Banerjee, *Interface Focus*, 2017, **7**, 20160128.
40 H. Xu, A. K. Das, M. Horie, M. S. Shaik, A. M. Smith, Y. Luo, X. Lu, R. Collins, S. Y. Liem, A. Song, P. L. A. Popelier, M. L. Turner, P. Xiao, I. A. Kinloch and R. V. Ulijn, *Nanoscale*, 2010, **2**, 960–966.
41 X. Zhang, R. Dai, H. Sun, Y. Zhang, D. Liu, M. Wang, M. Sun and H. Yu, *Mater. Chem. Front.*, 2020, **4**, 222–230.
42 A. Ajayaghosh and V. K. Praveen, *Acc. Chem. Res.*, 2007, **40**, 644–656.
43 B. Ma and R. Nussinov, *Proc. Natl. Acad. Sci. U. S. A.*, 2002, **99**, 14126–14131.
44 M. N. C. Zarycz and C. F. Guerra, *J. Phys. Chem. Lett.*, 2018, **9**, 3720–3724.
45 S. Qu and M. Li, *Tetrahedron*, 2008, **64**, 10890–10895.
46 Y. Ji, X. Yang, Z. Ji, L. Zhu, N. Ma, D. Chen, X. Jia, J. Tang and Y. Cao, *ACS Omega*, 2020, **5**, 8572–8578.
47 N. S. Myshakina, Z. Ahmed and S. A. Asher, *J. Phys. Chem. B*, 2008, **112**, 11873–11877.
48 H. Fan, H. Jiang, X. Zhu, Z. Guo, L. Zhang and M. Liu, *Nanoscale*, 2019, **11**, 10504–10510.
49 F. Arcudi, L. Đorđević and M. Prato, *Acc. Chem. Res.*, 2019, **52**, 2070–2079.
50 G. Ge, L. Li, D. Wang, M. Chen, Z. Zeng, W. Xiong, X. Wu and C. Guo, *J. Mater. Chem. B*, 2021, **9**, 6553–6575.
51 J. C. G. E. d Silva and H. M. R. Gonçalves, *TrAC, Trends Anal. Chem.*, 2011, **30**, 1327–1336.
52 M. L. Liu, B. B. Chen, C. M. Li and C. Z. Huang, *Green Chem.*, 2019, **21**, 449–471.
53 H. Wang, M. Zhang, Y. Ma, B. Wang, H. Huang, Y. Liu, M. Shao and Z. Kang, *ACS Appl. Mater. Interfaces*, 2020, **12**, 41088–41095.
54 A. I. Kasouni, T. G. Chatzimitakos, A. N. Troganis and C. D. Stalikas, *Mater. Today Commun.*, 2021, **26**, 102019.
55 L. Đorđević, F. Arcudi, A. D'Urso, M. Cacioppo, N. Micali, T. Bürgi, R. Purrello and M. Prato, *Nat. Commun.*, 2018, **9**, 3442.
56 M. Zhang, L. Hu, H. Wang, Y. Song, Y. Liu, H. Li, M. Shao, H. Huang and Z. Kang, *Nanoscale*, 2018, **10**, 12734–12742.
57 X. Miao, D. Qu, D. Yang, B. Nie, Y. Zhao, H. Fan and Z. Sun, *Adv. Mater.*, 2018, **30**, 1704740.
58 H. Ding, J. S. Wei, N. Zhong, Q. Y. Gao and H. M. Xiong, *Langmuir*, 2017, **33**, 12635–12642.
59 A. Sharma, T. Gadly, A. Gupta, A. Ballal, S. K. Ghosh and M. Kumbhakar, *J. Phys. Chem. Lett.*, 2016, **7**, 3695–3702.

